JOURNAL OF AIRCRAFT
Vol. 31, No. 6, November–December 1994

Computation of the Poststall Behavior of a Circulation Controlled Airfoil

Samuel W. Linton*
Sterling Software at NASA Ames Research Center, Moffett Field, California 94035

This article describes the numerical simulation of stalled and unstalled flows over a circulation controlled airfoil (CCA) using a fully implicit Navier-Stokes code, and the comparison with experimental results. Mach numbers of 0.3 and 0.5 and jet total to freestream pressure ratios of 1.4 and 1.8 are investigated. The Baldwin-Lomax and k-ε turbulence models are used, each modified to include the effect of strong streamline curvature. The numerical solutions of the poststall CCA show a highly regular unsteady periodic flowfield. This is the result of an alternation between adverse pressure gradient and shock-induced separation of the boundary layer on the airfoil trailing edge.

Nomenclature

a_∞ = freestream sound speed
C_p = pressure coefficient
c = chord length
c_l = sectional lift coefficient
c_μ = jet momentum coefficient, $(\dot{m}_j V_j^*/q_\infty S)$
M_∞ = freestream Mach number
$\dot{m}_j$ = jet mass flux
q_∞ = freestream dynamic pressure
Re_∞ = freestream Reynolds number
Ri_t = turbulent Richardson number
S = wing planform area
T = period of oscillation
$\hat{T}$ = nondimensional period, (Ta_∞/c)
t = time
$\hat{t}$ = nondimensional time, (ta_∞/c)
V_j^* = characteristic jet velocity
μ_t = eddy viscosity

Introduction

A CONVENTIONAL airfoil has a sharp trailing edge, which is an efficient mechanism for fixing circulation. However, the lift generated by such an airfoil cannot be directly controlled, but is a function of angle of attack and freestream velocity. Also, the maximum lift coefficient that can be obtained is quite limited, because the adverse pressure gradient on the upper surface that increases with lift causes boundary-layer separation and stall.

The circulation controlled airfoil[1–21] (CCA) overcomes these drawbacks with a rounded trailing edge—called a Coanda surface—along which the rearward stagnation point is free to move, and an upper surface jet near the trailing edge to energize the boundary layer (Fig. 1). Since the jet blowing rate is regulated, the separation point is controlled, and thereby the circulation and lift. An additional benefit for high-lift applications is that, because of the delayed separation of the boundary layer near the trailing edge, a very high maximum lift coefficient can be obtained (greater than 6 is not unusual at low freestream Mach numbers).

The variation of CCA lift with c_μ is highly nonlinear, and is strongly affected by other parameters such as angle of attack, Mach number, and trailing-edge geometry.[11] However, a generalization can be made that for low blowing rates, $c_l \sim c_\mu$, and for high blowing rates $c_l \sim \sqrt{c_\mu}$.[13] Eventually, however, the lift augmentation with c_μ ceases. This phenomena, which is unique to CCAs, is known as jet stall, defined as the condition at which $dc_l/dc_\mu = 0$.

There are two forms of jet stall for a CCA. The first, called jet detachment stall, is due to the premature separation of the jet from the Coanda surface. This causes an immediate loss in the suction over the trailing edge, and a sharp drop in lift. This form of jet stall can probably be avoided with proper design of the airfoil, and is not the topic of this article.

The second kind of jet stall, known as C_p^* stall, appears to be inevitable, and, as originally described by Abramson and Rogers,[2] seems to begin soon after the first occurrence of critical pressure (the pressure at which sonic flow will develop) on the Coanda surface. This stall is marked by a relatively gradual loss of suction over the entire upper surface, without the jet separation or precipitous loss of suction on the Coanda surface that characterizes jet detachment stall. Consequently, the drop in lift is relatively gradual. Experimentalists have also observed that the wake becomes very unsteady in this form of stall.

Because a primary use for the CCA is as a high-lift device, understanding its behavior at stall is crucial to its effective

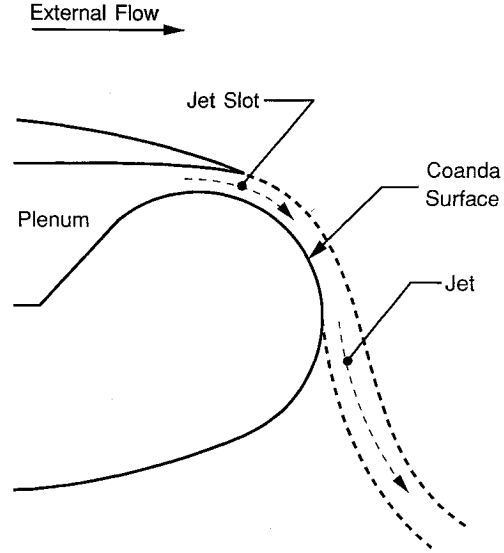

Fig. 1 Schematic of a CCA.

Presented as Paper 93-0207 at the AIAA 31st Aerospace Sciences Meeting and Exhibit, Reno, NV, Jan. 11–14, 1993; received July 26, 1993; revision received Feb. 3, 1994; accepted for publication Feb. 3, 1994.

*Research Scientist, M/S T027B-2. Member AIAA.

and safe use. Although Wood[11] has described C_p^* stall as the result of a breakdown in mixing between the jet and outer flow, the exact mechanism involved has not been previously identified. The need to understand this provides the impetus for the present numerical study of a C_p^*-stalled CCA.

Governing Equations

The Reynolds-averaged Navier-Stokes equations were used in the present simulation. The turbulence models used were the Baldwin-Lomax[22] and Jones-Launder[23,24] k-ε models, both modified to include the effects of the strong streamline curvature[25,26] that occur, particularly over the Coanda surface.

The Baldwin-Lomax model uses algebraic relations to solve for μ_t. The curvature correction used was that suggested by Baldwin et al.,[27] and implemented by Pulliam et al.[28] It entails a direct correction to the eddy viscosity based on the local radius of curvature of the streamlines. A single constant, C_c is specified. Although Pulliam et al. tuned this constant on a case by case basis, a single value of 2.0 was used herein.

In the present research, the k-ε equations were integrated to the wall, and the curvature correction given by Launder et al.[29] was used. This method involves the multiplication of the ε decay term by a linear function of Ri_t.

Numerical Method

The numerical method used was a fully implicit, second-order accurate in space, finite volume technique. The differencing of the Euler terms was accomplished by using MacCormack's modification of Steger-Warming flux-splitting[30-33]. The viscous terms were differenced using standard central differences. The implicit treatment of the source terms in the k-ε equations was done in a novel way,[41] designed to increase robustness, particularly when the time scales involved were much shorter than those of the fluid flow.

For steady-state solutions, and during the initial transients of the time-accurate problems, local time stepping was used to speed the computations. In addition, a separate time step was used for the k-ε equations, which was scaled by the time scales of the source terms. This, too, was found to increase the efficiency and robustness of the numerical method.

On the CCA body, simple no-slip boundary conditions were used. The use of an O-grid about the body necessitated periodic boundary conditions. Along the jet inflow boundary, the total pressure, total temperature, and flow direction were specified, and the remaining quantity was derived from the appropriate characteristic relation.[34] Similarly, in the far field, the appropriate quantities were derived from the interior from the outflowing characteristic relations, and freestream values were used for the remaining quantities.

The system of equations for the change in the conservation variables that resulted at each time step was solved using back-and-forth line Gauss-Seidel iteration. All unknowns that exceeded the block-tridiagonal bandwidth, however, were moved to the "right-hand-side" of the equation, so that their latest available values were used at every iteration. Typically, two back-and-forth iterations were used at each time step. It was verified that the unsteady solutions were insensitive to further sweeps.

Configuration and Parameters

The computations corresponded to the experiments of Keener et al.[20] They obtained pressure measurements only on an unswept semispan wing of aspect ratio 4 in the NASA Ames Research Center 6- × 6-ft Transonic Wind Tunnel. Inboard on the wing, the flowfield was approximately two dimensional, justifying the present two-dimensional computations.

The CCA in the computations was the wing section used in the experiment. It was based on a 20% thick ellipse, modified with 4% radius circular leading and trailing edges. The jet slot was placed at 96.7% chord and had a nominal slot height of 0.002 chords with a lip thickness of 0.0008 chords.

The computations were performed at Mach numbers of 0.3 and 0.5, with corresponding Reynolds numbers of 1.7×10^6 and 2.6×10^6. The jet total to freestream pressure ratios used were 1.4 and 1.8. Three grids of increasing resolution were used where appropriate for grid sequencing, and a fourth very fine grid for a grid refinement study. The k-ε and Baldwin-Lomax turbulence model results were compared.

Grid

The construction of a high-quality grid about the CCA is made difficult by the presence of the jet channel that originates in an interior plenum. Shrewsbury[35-37] and Willians and Franke[38] solved this problem by treating the jet slot as a grid boundary. Pulliam et al.[28] used an innovative spiral grid topology as well as a multiblock strategy. Viegas et al.[39] used a strip of cells of vanishing volume along the body. Finally, Berman[40] used a nonrectangular computational domain.

In the present research a technique similar to that of Viegas and Berman was used. First, the jet region was "faired" over, making a closed inner boundary. The outer boundary of the grid was a circle centered at the airfoil midchord, 25 chord lengths in radius. An O-grid was constructed between these two boundaries using an elliptic grid generator. Then, the grid within the jet channel up to the slot was formed, also with an elliptic grid generator. Finally, these two portions of the grid were merged, and a strip of cells of vanishing volume were added in the cusped region bounded by the jet slot and lip, the Coanda surface, and the inside of the fairing. Note that the result is not a rectangular domain in computational space. However, the present computer codes are able to accommodate such a region without the need for a multiblock scheme.

The fine grid, which has dimensions of 255 × 210 volumes, is shown in Fig. 2. The medium grid with dimensions of 127 × 105 and the coarse grid with dimensions of 64 × 53 were both interpolated from the fine grid, and were used for grid sequencing. Finally, the very fine grid generated for the grid refinement study had dimensions of 355 × 293.

Details of the Computation

In the computations it was found that the jet mass flow obtained at a given pressure ratio was uniformly lower than that obtained in the experiment. It is possible that the jet slot height varied from its nominal value in the experiments, due either to being set inexactly, or due to expansion from the high plenum pressures within the jet channel. This same effect has been noted by other researchers (e.g., Pulliam et al.[28]). Thus in the computations, a jet slot height about 15% higher than the nominal value was used in order to match the jet momentum coefficient more closely.

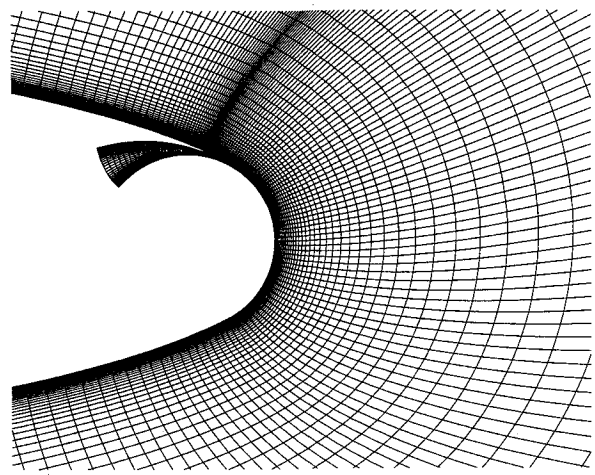

Fig. 2 Detail of the trailing edge of the fine grid (255 × 210).

One complication in choosing the conditions for the two-dimensional computations is that the experiment was performed on a finite three-dimensional wing. A two-dimensional computation is an acceptable model of such a flow if, as was the case for the steady flows in this research, the sectional lift coefficient on the wing varies slowly over the wing, so that the flow is very nearly two dimensional. However, the finite wing induces downwash along the span. This downwash is not known a priori, and cannot be accurately computed from the experimental sectional lift coefficients provided at only five stations. Thus, the angle of attack was varied in the two-dimensional computation until the pressure coefficient matched that of the experiment as closely as possible.

There are two problems with this technique. First, the error in the lift coefficient at the correct induced angle of attack cannot be determined. Secondly, the need to compute multiple angles of attack greatly increases the cost of the computation at a single desired lift coefficient, particularly since the lift curve slope of a CCA is nonlinear. Thus, a single solution represents multiple trial computations at various angles of attack. In order to minimize the considerable computational expense of this process, these trials were performed on the coarse grid with the Baldwin-Lomax model. Once the angle of attack had been optimized on the coarse grid, the same angle was used for all other computations of that case. It was found that the flowfields computed on the coarse, medium, and fine grids were all qualitatively the same, with a difference in lift of less than 20%.

In order to estimate the actual error in lift predictions without having to specify an angle of attack, some three-dimensional computations were performed as well.[41] These computations were also useful in verifying the local two-dimensionality of the flowfield inboard of the wingtip. However, these computations, which were performed on a three-dimensional version of the coarsest grid with the modified Baldwin-Lomax model only, should be considered preliminary.

The use of boundary-layer control to fix the location of the rearward stagnation point on a CCA makes it a uniquely challenging computation. The reason for this is the notorious weakness of turbulence models applied to flowfields near separation and under the influence of streamline curvature. The resulting error in predicting the separation location has a dramatic effect not only on the flow over the Coanda surface, but, since it determines the lift, on the global flowfield as well. This implies that it is more difficult to obtain the very good agreement between computation and experiment that is possible for unstalled conventional airfoils, for which the boundary-layer effects are of a higher order only.

Unstalled Results

The first group of computations were those for which the CCA was unstalled, and the resulting flowfields were steady. The pressure coefficient distribution for the CCA at a Mach number of 0.3 and a pressure ratio of 1.4 is shown in Fig. 3. This result is from a Baldwin-Lomax computation on the fine grid. The computed jet momentum coefficient was 0.023, and the lift coefficient was 1.27, in comparison with the experimental values of 0.024 and 1.48, respectively. The pressure distribution computed at an angle of attack of −4.5 deg matches that of the experiment well, except near the leading edge, where the suction peak is underpredicted. This is at least partially due to the difference in lift predicted by the coarse and fine grid solutions. This pressure distribution, which is quite typical of a CCA, has a very flat pressure distribution over the majority of the upper surface due to its elliptic shape. Similarly, the lower surface pressure is quite flat. The discontinuity in the derivative of the slope of the surface between the circular leading edge and the elliptic portion of the airfoil results in a small disturbance in the pressure. The most unique feature of the pressure coefficient distribution is the very severe suction peak on the upper surface near the trailing edge

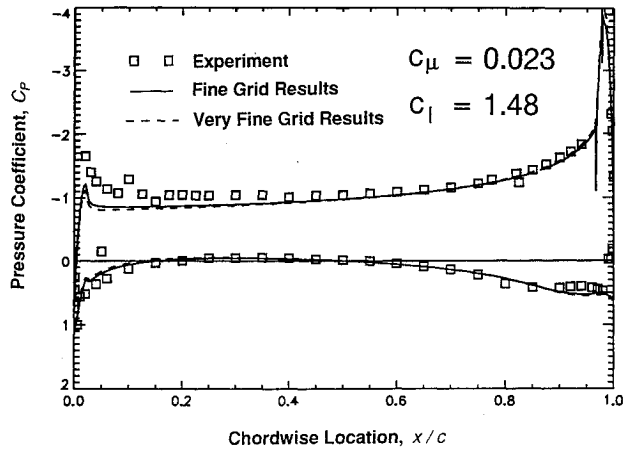

Fig. 3 Pressure distribution at M_∞ = 0.3, pressure ratio = 1.4, predicted by the Baldwin-Lomax model on the fine and very fine grids.

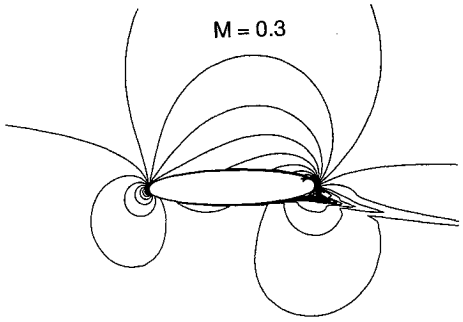

Fig. 4 Mach number contours predicted by the Baldwin-Lomax model at M_∞ = 0.3, pressure ratio = 1.4.

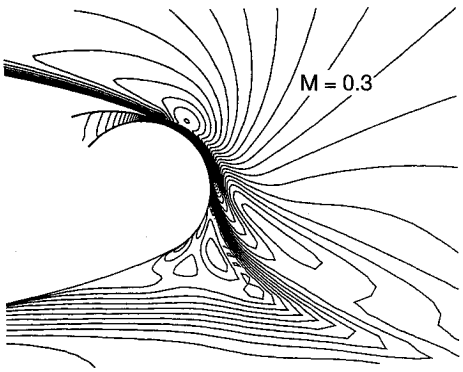

Fig. 5 Detail of the Mach number contours over the Coanda surface predicted by the Baldwin-Lomax model at M_∞ = 0.3, pressure ratio = 1.4.

due to the jet exhausting onto the Coanda surface. Notice that the pressure on the upper surface begins to drop ahead of the jet slot, indicating that the exterior flow is accelerated upstream.

The Mach number contours over the airfoil corresponding to this case are displayed in Fig. 4. The plot shows a stagnation point below the centerline on the leading edge consistent with a lifting airfoil. The upper surface contours show once again that the jet begins to accelerate the flow well forward of the jet slot. Aft of the airfoil the velocity profile of the jet is evident.

The Coanda surface flow, which causes the suction peak, is shown in Fig. 5. This plot shows the acceleration of the jet from near stagnation conditions within the airfoil plenum up to a maximum Mach number of about 0.93. This high-velocity

fluid travels along the Coanda surface until it separates on its lower section. The jet also accelerates the external flow through entrainment. This entrainment at the slot and downstream of it creates a favorable pressure gradient that provides for the additional acceleration of the upstream external flow.

For the second two-dimensional run, the pressure in the jet plenum was raised to 1.8 times the freestream pressure. This resulted in a jet momentum coefficient of $c_\mu = 0.042$ and a lift coefficient of 2.21, compared to the experimental values of 0.046 and 2.21, respectively. Figure 6 shows the pressure coefficient for this case computed on a fine grid with the Baldwin-Lomax model. The angle of attack that optimized the fit on the coarse grid was −5.0 deg. The fit to the data is excellent, including the leading-edge suction peak, as well as the jet suction values. Qualitatively, the results are similar to those obtained at pressure ratio of 1.4, although the higher jet velocity creates a much greater suction peak at the slot.

Figure 7 is the Coanda surface Mach contour plot for this case. It is similar to Fig. 5, except that the jet leaves the airfoil at a steeper downward angle, as is consistent with the increased lift. Also, the jet accelerates to a higher Mach number of about 1.35 on the Coanda surface, and remains attached farther along it.

Both of the above cases were computed using the Baldwin-Lomax model with the streamline curvature correction term. In order to compare the performance of the two turbulence models and their respective curvature corrections, these two cases were also run on the fine grid with the modified k-ε model.To enable a direct comparison, the same angles of attack were used as in the corresponding Baldwin-Lomax model computations. The results for the 1.4 pressure ratio case was a lift coefficient about 50% higher than that of the Baldwin-Lomax model. The same pattern was seen in the comparison of the 1.8 pressure ratio k-ε computation with the corresponding Baldwin-Lomax computation.

It should be noted that since the angle of attack for each run was chosen to optimize the fit of the Baldwin-Lomax coarse grid solution to the experiment, the two-dimensional results alone cannot be used to determine which of the turbulence models is the most accurate. However, preliminary coarse grid three-dimensional computations[41] indicate that the Baldwin-Lomax model with the corresponding streamline curvature correction overpredicts the lift on the CCA (by about 17%). Thus, insofar as the current modified k-ε model uniformly predicts higher lift than the Baldwin-Lomax model, the author would speculate that for these cases, the Baldwin-Lomax model gives more accurate values for lift. However, since the curvature corrections are highly dependent on the specific parameters of the flowfield, it is incorrect to infer that the Baldwin-Lomax model will always give more accurate answers. Furthermore, a more accurate lift prediction implies a better separation point location, but not necessarily a better prediction of the details of the turbulent boundary layers. Regardless, the current accuracy estimates should be verified by higher resolution three-dimensional computations.

To estimate the grid dependency of the two-dimensional solutions, the computation at a Mach number of 0.3 and a pressure ratio of 1.4 was repeated on the very fine grid. The lift coefficient was found to agree to within 0.8%. The resulting pressure profile is compared with that of the fine grid in Fig. 3.

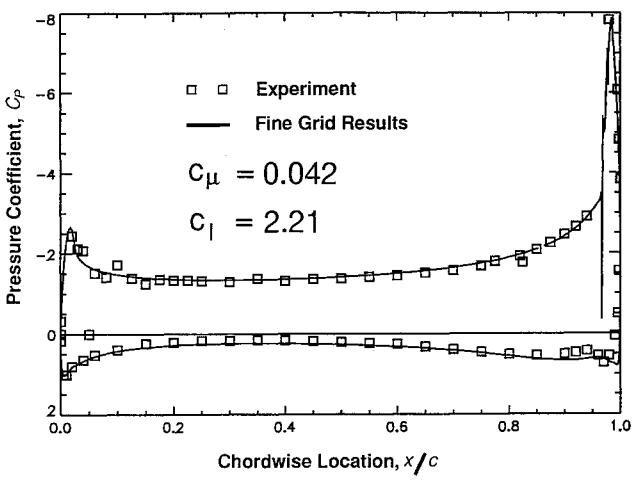

Fig. 6 Pressure distribution at M_∞ = 0.3, pressure ratio = 1.8, predicted by the Baldwin-Lomax model on the fine grid.

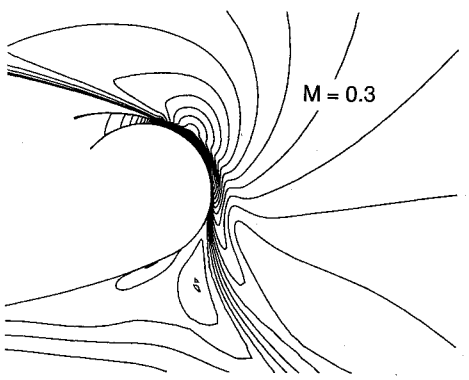

Fig. 7 Detail of the Mach number contours over the Coanda surface predicted by the Baldwin-Lomax model at M_∞ = 0.3, pressure ratio = 1.8.

Stalled Results

Previously, a time-accurate computation about a CCA has been performed by Shrewsbury and Sankar,[37] who computed the flow over a pitching airfoil. However, the present research is the first known time-accurate computation and explanation of the unforced C_p^* stall mechanism of CCAs.

Figure 8 is a plot of the computed mean lift coefficient of the airfoil at a Mach number of 0.5 and angle of attack of −5.4 deg, as a function of jet momentum coefficient. At a value of about 0.013, corresponding to a pressure ratio of 1.8, the airfoil is stalled. Beyond stall, computations of the CCA flowfield revealed a self-sustained unsteady flowfield. Thus, the minimum and maximum values of the lift are also plotted as well.

In order to explain the mechanism of stall, the results of the computation for the pressure ratio of 1.8 will be described. Figure 9 shows roughly one cycle of the lift coefficient vs $\hat{t}$.

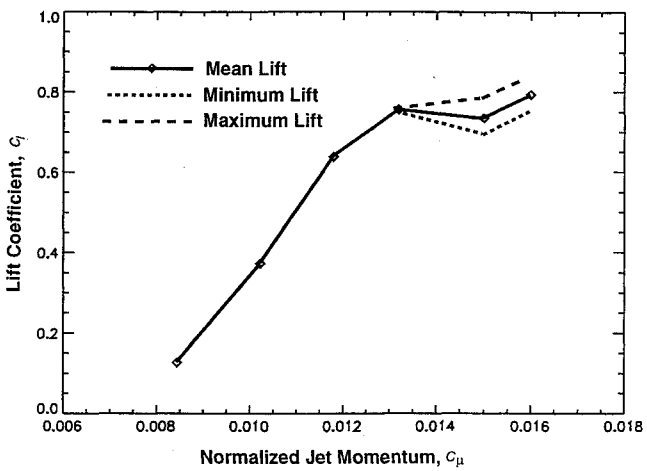

Fig. 8 Lift coefficient as a function of jet momentum coefficient, computed with the Baldwin-Lomax model on the coarse grid, M_∞ = 0.5.

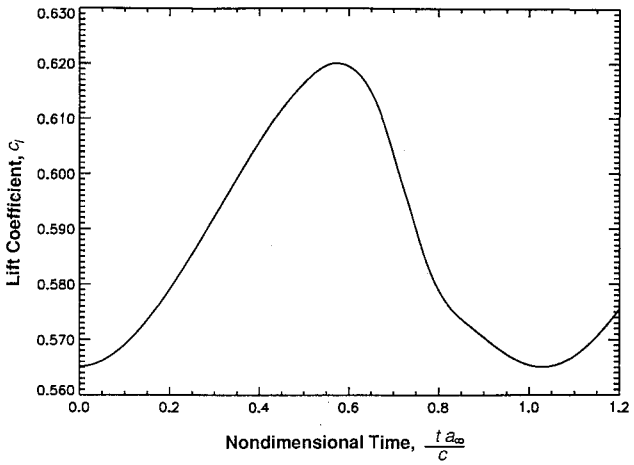

Fig. 9 Lift coefficient as a function of nondimensional time for the stalled case.

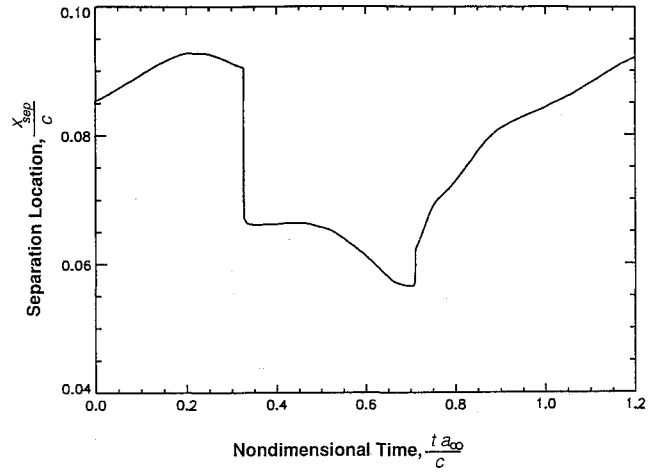

Fig. 10 First separation point distance from jet slot normalized by chord length, as a function of nondimensional time for the stalled case.

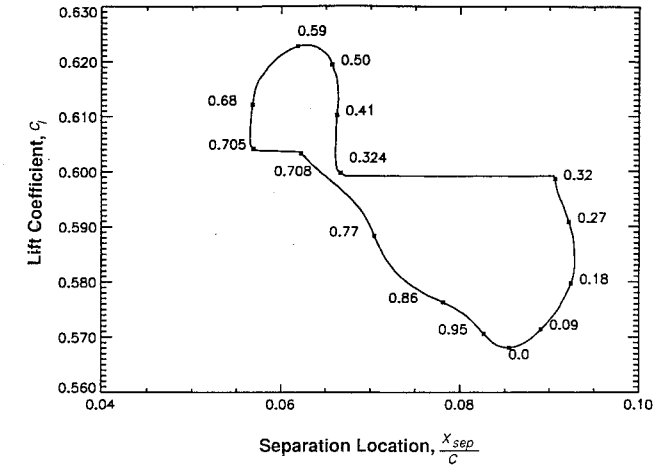

Fig. 11 Phase plane diagram, with points labeled with nondimensional time.

The unsteadiness was found to be periodic and remarkably regular. In physical units, the frequency corresponding to a $\hat{T}$ of 1.0 was about 1 kHz for the experiment of Keener et al.[20] Since the lift coefficient is intimately connected with the separation point location on the Coanda surface, the distance of the first such point from the jet slot, normalized by chord, is plotted in Fig. 10. It has the anticipated periodic nature, but has an unexpected discontinuity as well. Another way to plot the two variables is against each other, rather than as functions of time, so that a phase plane diagram results (Fig. 11). In this figure, various points are labeled with the nondimensional time corresponding to Figs. 9 and 10. The paths followed by multiple cycles plotted in this way overlap each other, indicating that the oscillation is indeed highly regular, and that initial transients have died away.

This unsteadiness results from the alternation of jet boundary-layer separation on the Coanda surface between two distinct mechanisms. The usual cause of separation is the adverse pressure gradient due to the rearward stagnation point on the trailing edge. In addition, however, when the jet and entrained external flow are accelerated to a sufficiently high supersonic velocity, a shock forms. The adverse pressure gradient across this shock causes massive separation. The unsteadiness is a result of the alternation of the mechanism of jet separation between these two types, and the phase lag between the change in the flow over the Coanda surface, and the establishment of the resulting pressure field over the full airfoil.

Figures 12a–12f, which show the Coanda surface Mach contours at selected instants in the cycle, illustrate this process. From $\hat{t} = 0$ (Fig. 12a) to 0.18, the wall jet Mach number increases, and the separation point moves down along the Coanda surface. As expected, the lift increases as well. From $\hat{t} = 0.27$ to 0.34, the separation point has stopped its downward motion, and has actually begun to recede slightly, probably due to the increasingly adverse pressure gradient at the higher lift. However, because the development of the lift lags the separation point movement, the lift continues to increase. This lag occurs because the change in the pressure of the external flow triggered by jet entrainment takes a finite length of time to travel upstream.

Figures 10 and 11 show that a sudden change occurs in the location of the first separation point between $\hat{t} = 0.32$–0.324. This is the result not of movement of the separation point, but of the formation of a new one closer to the jet slot due to the increasingly adverse pressure gradient. Even so, the lift continues to increase.

At $\hat{t} = 0.41$ (Fig. 12b), the low pressure on the Coanda surface at the high lift continues to accelerate the jet, and, due to its entrainment, a small pocket of the external flow becomes supersonic. The lift continues to grow.

At $\hat{t} = 0.50$ (Fig. 12c), a weak shock forms in the high-velocity region of the jet, and extends a small distance into the external flowfield.

The continued acceleration of the jet between $\hat{t} = 0.50$ (Fig. 12c) and 0.59 (Fig. 12d) due to the sustained growth of the lift causes the shock to strengthen and move forward on the Coanda surface, so that the separation point location also moves forward. The shock then causes a large separation bubble to form (Fig. 12d), with reattachment farther down on the Coanda surface. At this instant, the lift reaches its maximum value, and, lagging the separation point movement, subsequently begins to decrease. At $\hat{t} = 0.68$ (Fig. 12e), the separation bubble bursts, shedding vortices into the wake. This causes the shock to dissipate, but a pressure pulse is formed that travels upstream. At this point, the jet separation point is at its farthest upstream.

Between $\hat{t} = 0.705$–0.708, the jet rapidly reattaches, causing another sudden change in the separation location. The shed vortices are convected downstream, and the separation point resumes its movement down the Coanda surface (Fig. 12f). In addition, there seems to be another high-pressure wave sent upstream due to the transient obstruction posed by the bursting separation bubble. Once the lagging lift bottoms out, the flowfield returns to its original state, and the process repeats.

This computation was also performed using the k-ε turbulence model. The result had the same characteristics as the Baldwin-Lomax model solution, despite the significantly higher

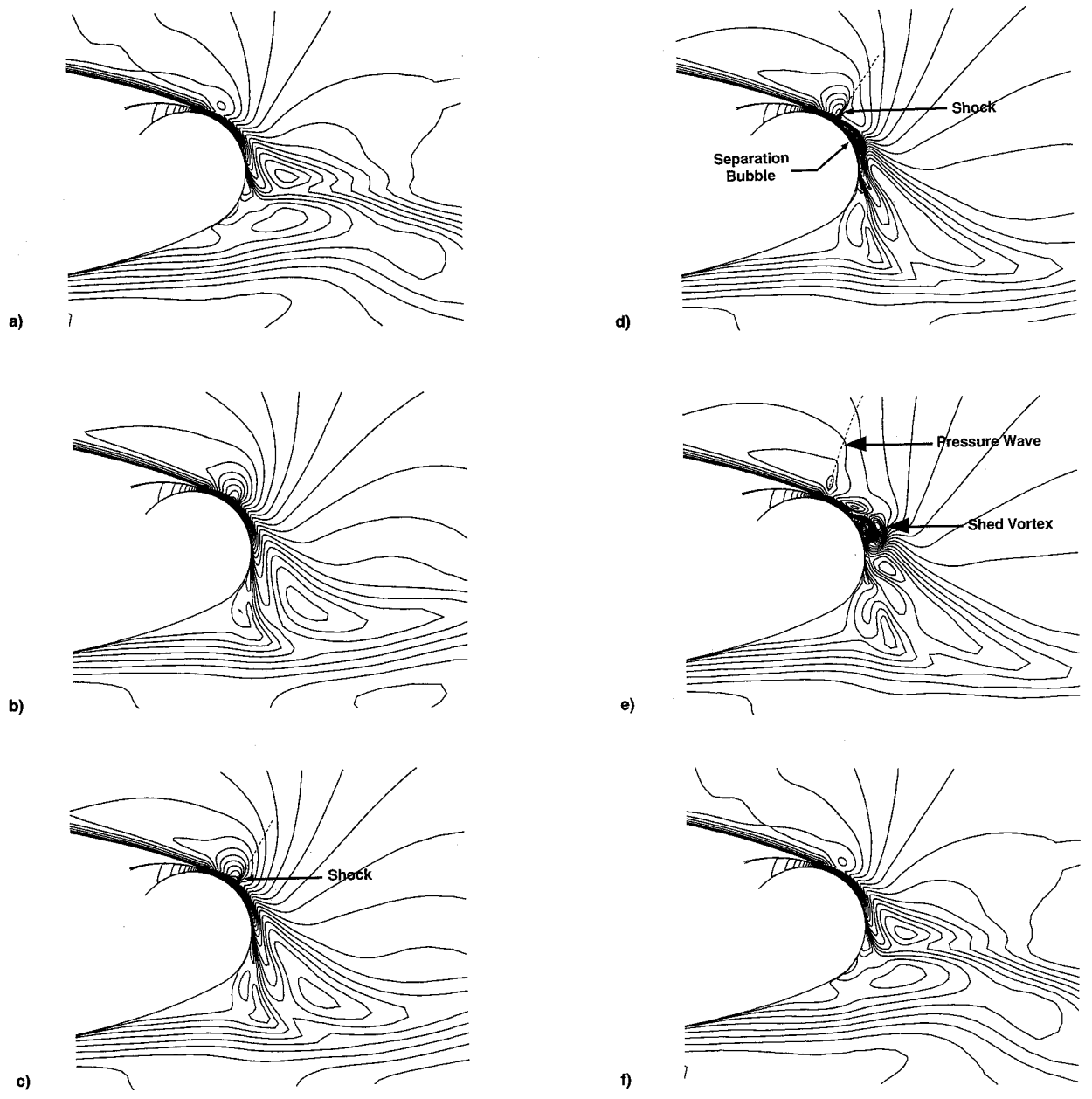

Fig. 12 a) Stalled flowfield Mach contours, $\hat{t} = 0.00$, the separation point moves down the Coanda surface; b) $\hat{t} = 0.41$, supersonic flow develops; c) $\hat{t} = 0.50$, a shock forms on the Coanda surface; d) $\hat{t} = 0.59$, the strengthening shock causes the jet to form a separation bubble; e) $\hat{t} = 0.68$, the separation bubble bursts, and vorticity is released into the freestream; and f) $\hat{t} = 0.86$, the jet rapidly reattaches, and the separation point moves down the Coanda surface.

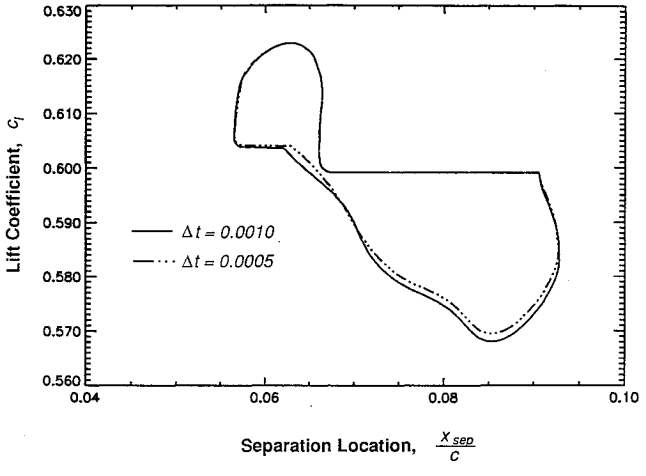

Fig. 13 Comparison of the phase plane plot at two different time steps.

mean lift coefficient and longer period (by about 25%) it predicted. This verifies that the stall mechanism is not due to a peculiarity of the Baldwin-Lomax model.

In order to verify that the correct time-dependent behavior was captured, the computations were repeated with reduced time steps. For the coarsest grid, the time step was halved three times for three additional computations, with essentially identical results. This of course was impractical on the fine grid. (Each cycle of the computation takes about an hour at the typical time step, and as many as 10 cycles were required for the transients to die out.) However, Fig. 13 shows the phase diagram obtained on the fine grid with the typical non-dimensional time step, 0.0010, as well as that obtained with a time step of 0.0005. The comparison is quite good, and implies that the time step of 0.001 is adequately small to achieve temporal accuracy.

The present computations of stall cannot be compared directly to the experiments of Keener and Spaid for several reasons. First of all, whereas a steady two-dimensional computation can model the flow over a wing at a fixed spanwise

station if the induced angle of attack is selected correctly, this is not true for an unsteady flow. The reason for this is that the upwash induced along a three-dimensional wing with time-varying lift is unsteady. There is really no way to simulate this effect without quite detailed information about the three-dimensional experimental flowfield. Secondly, the instrumentation used in the experiment was incapable of measuring the flow unsteadiness predicted computationally, since its time-response was significantly slower than that needed to resolve oscillations on the order of a kilohertz.

There is evidence that supports the present explanation of C_p^* jet-stall, however. First of all, as demonstrated by Fig. 10, the mechanism discovered here occurs when $dc_l/dc_\mu \approx 0$, which is the definition of jet stall. It explains why subsequent increases in the pressure ratio fail to increase the lift: the higher total pressure of the jet increases its Mach number on the Coanda surface, thus resulting in progressively stronger shocks. These shocks cause massive separation that destroys the ability of the jet to establish circulation and lift.

The present mechanism explains why the appearance of the critical pressure on the Coanda surface precedes stall,[2] since a shock is necessary to cause the separation near the jet slot. It also explains why, as observed experimentally, stall occurs at lower blowing rates for higher Mach numbers: an equivalent jet to freestream velocity ratio at a higher freestream Mach number implies a higher jet Mach number.

Finally, numerous CCA researchers have noticed a correlation between stall and unsteady flow.

Concluding Remarks

The present research is the first numerical investigation of the CCA C_p^* stall. The two-dimensional computations uncovered a highly regular periodic oscillation due to the alternation between adverse pressure gradient separation and shock-induced separation of the jet boundary layer on the Coanda surface. Although there is substantial evidence that this is the actual mechanism of stall, experimental verification is needed. In addition, high resolution three-dimensional computations are needed to allow more direct comparison to experiment.

Although both turbulence models used gave qualitatively the same results both for stalled and unstalled airfoils, the quantitative results showed extreme sensitivity to the turbulence model and the corresponding streamline curvature correction. Because of the role of the models in determining the separation point location on the trailing edge, this resulted in large discrepancies in the computed lift. Clearly, further research is required into the modeling of turbulence in flows with severe streamline curvature, particularly near separation.

Acknowledgment

The present work was supported by the NASA Ames University Consortium Office Interchange for Joint Research, Moffett Field, California, Contract NCA-2-259.

References

[1]Abramson, J., "Two Dimensional Subsonic Wind Tunnel Evaluation of a 20 percent Thick Circulation Control Airfoil," David Taylor Naval Ship Research and Development Center, DTNSRDC Rept. ASED 311, Bethesda, MD, 1975.

[2]Abramson, J., and Rogers, E. O., "High-Speed Characteristics of Circulation Control Airfoils," AIAA Paper 83-0265, Jan. 1983.

[3]Englar, R. J., "Circulation Control for High Lift and Drag Generation on STOL Aircraft," *Journal of Aircraft*, Vol. 12, No. 5, 1975, pp. 457–463.

[4]Englar, R. J., and Applegate, C.A., "Circulation Control—An Updated Bibliography of DTNSRDC Research and Selected Outside References," David Taylor Naval Ship Research and Development Center, DTNSRDC Rept. 84-052, Bethesda, MD, 1984.

[5]Englar, R. J., "Development of Circulation Control Technology for Powered-Lift STOL Aircraft," *Proceedings of the Circulation Control Workshop*, 1986, pp. 491–538 (NASA CP-2432).

[6]Franke, M. E., and Harvell, J. K., "Wind Tunnel Studies of Circulation Control Elliptical Airfoils," *Proceedings of the Circulation Control Workshop*, 1986, pp. 267–288 (NASA CP-2432).

[7]Jones, D. G., "The Performance of Circulation Controlled Airfoils," Ph.D. Dissertation, Cambridge Univ., Cambridge, England, UK, 1970.

[8]Stevenson, T. A., Franke, M. E., Rhynard, W. E., Jr., and Snyder, J. R., "Wind Tunnel Study of a Circulation-Controlled Elliptical Airfoil," *Journal of Aircraft*, Vol. 14, No. 9, 1977, pp. 881–886.

[9]Wood, N. J., "The Aerodynamics of Circulation Control Aerofoils," Joint Inst. for Aeronautics and Acoustics TR-41, 1981.

[10]Wood, N. J., and Conlon, J. A., "The Performance of a Circulation Control Airfoil at Transonic Speeds," AIAA Paper 83-0083, Jan. 1983.

[11]Wood, N. J., "Circulation Control Airfoils: Past, Present Future," AIAA Paper 85-0204, Jan. 1985.

[12]Wood, N. J., "The Further Development of Circulation Control Airfoils," *Proceedings of the Circulation Control Workshop*, 1986, pp. 183–198 (NASA CP-2432).

[13]Loth, J. L., "Circulation Control STOL Aircraft Design Aspects,"*Proceedings of the Ciruculation Control Workshop*, 1986, pp. 569–590 (NASA CP-2432).

[14]Nichols, J. H., and Harris, M. J., "Fixed Wing CCW Aerodynamics with and Without Supplementary Thrust Deflection," *Proceedings of the Circulation Control Workshop*, 1986, pp. 479–490 (NASA CP-2432).

[15]Nielsen, J. N., and Biggers, J. C., "Recent Progress in Circulation Control Aerodynamics," AIAA Paper 87-0001, Jan. 1987.

[16]Novak, C. J., and Cornelius, K. C., "Investigations of a Circulation Control Airfoil Flowfield Using an Advanced Laser Velocimeter," *Proceedings of the Circulation Control Workshop*, 1986, pp. 71–98 (NASA CP-2432).

[17]Novak, C. J., Cornelius, K. C., and Roads, R. K., "Experimental Investigations of the Circular Wall Jet on a Circulation Control Airfoil," AIAA Paper 87-0155, Jan. 1987.

[18]Rodman, L. C., and Wood, N. J., "Verification of Performance Results for a Low-Speed 15% Elliptical Circulation Control Airfoil," JIAA TR-56, 1986.

[19]Spaid, F. W., and Keener, E. R., "Boundary-Layer and Wake Measurements on a Swept Circulation-Control Wing," *Proceedings of the Circulation Control Workshop*, 1986, pp. 239–266 (NASA CP-2432, Feb. 1986.

[20]Keener, E. R., Sanderfer, D. T., and Wood, N. J., "Pressure Distributions and Oil-Flow Patterns for a Swept Circulation-Control Wing," *Proceedings of the Circulation Control Workshop*, 1986, pp. 209–238 (NASA CP-2432).

[21]Kind, R. J., "A Proposed Method of Circulation Control," Ph.D. Dissertation, Cambridge Univ., Cambridge, England, UK, 1967.

[22]Baldwin, B. S., and Lomax, H., "Thin Layer Approximation and Algebraic Model for Separated Turbulent Flows," AIAA Paper 78-257, Jan. 1978.

[23]Launder, B. E., and Spaulding, D. B., "The Numerical Computation of Turbulent Flows," *Computer Methods in Applied Mechanics and Engineering*, Vol. 3, 1974, pp. 269–289.

[24]Jones, W. P., and Launder, B. E., "The Prediction of Laminarization with a Two-Equation Model of Turbulence," *International Developments in Heat Transfer*, Vol. 15, 1972, pp. 303–314.

[25]Bradshaw, P., "Effects of Streamline Curvature on Turbulent Flow," AGARDograph 169, 1973.

[26]Bradshaw, P., "The Analogy Between Streamline Curvature and Buoyancy in Turbulent Shear Flow," *Journal of Fluid Mechanics*, Vol. 36, Pt. 1, 1969, pp. 177–191.

[27]Baldwin, B. S., Chigier, N. A., and Sheaffer, Y. S., "Decay of Far-Flowfield in Trailing Vortices," *AIAA Journal*, Vol. 11, No. 12, 1973, pp. 1601, 1602.

[28]Pulliam, T. H., Jespersen, D. C., and Barth, T. J., "Navier-Stokes Computations for Circulation Controlled Airfoils," AIAA Paper 85-1587, Jan. 1985.

[29]Launder, B. E., Priddin, C. H., and Sharma, B. I., "The Calculation of Turbulent Boundary Layers on Spinning and Curved Surfaces," *Journal of Fluids Engineering*, Vol. 99, 1977, p. 231.

[30]Steger, J. L., and Warming, R. F., "Flux Vector Splitting of the Inviscid Gasdynamic Equations with Application to Finite Difference Methods," NASA TM-78605, July 1979.

[31]MacCormack, R. W., "Current Status of Numerical Solutions of the Navier-Stokes Equations," AIAA Paper 85-0032, Jan. 1985.

[32]MacCormack, R. W., "Solution of the Navier-Stokes Equations in Three Dimensions," AIAA Paper 90-1520, Jan. 1990.

[33]Candler, G. V., and MacCormack, R. W., "Hypersonic Flow

Past 3-D Configurations," AIAA Paper 87-0480, Jan. 1987.
[34]Chakravarthy, S., "Euler Equations—Implicit Schemes and Boundary Conditions," AIAA Paper 82-0228, Jan. 1982.
[35]Shrewsbury, G. D., "Evaluation of Research Circulation Control Airfoil Using Navier-Stokes Methods," *Proceedings of the Circulation Control Workshop*, 1986, pp. 115–134 (NASA CP-2432).
[36]Shrewsbury, G. D., "Numerical Study of a Research Circulation Control Airfoil Using Navier-Stokes Methods," *Journal of Aircraft*, Vol. 26, No. 1, 1989, pp. 29–34.
[37]Shrewsbury, G. D., and Sankar, L., "Dynamic Stall of Circulation Control Airfoils," AIAA Paper 90-0573, Jan. 1990.
[38]Williams, S. L., and Franke, M. E., "Navier-Stokes Methods to Predict Circulation Control Airfoil Performance," *Journal of Aircraft*, Vol. 29, No. 2, 1992, pp. 243–249.
[39]Viegas, J. R., Rubesin, M. W., and MacCormack, R. W., "On the Validation of a Code and a Turbulence Model Appropriate to Circulation Control Airfoils," NASA TM-100090, April 1988.
[40]Berman, J. A., "A Navier-Stokes Investigation of a Circulation Control Airfoil," AIAA Paper 85-0300, Jan. 1985.
[41]Linton, S. W., "The Numerical Simulation of Circulation Controlled Airfoil Flowfields," Ph.D. Dissertation, Dept. of Aeronautics and Astronautics, Stanford Univ., Stanford, CA, 1992.